Statics and dynamics of interlayer interactions in the dense high-pressure graphite compound LiC_2

Chetna Bindra
Department of Physics and Laboratory for Research on the Structure of Matter, University of Pennsylvania, Philadelphia, Pennsylvania 19104

Vera A. Nalimova and Dmitry E. Sklovsky
Department of Chemistry, Moscow State University, Moscow 119899, Russia

William A. Kamitakahara
Reactor Radiation Division, National Institute of Standards and Technology, Gaithersburg, Maryland 20899

John E. Fischer
Department of Materials Science and Engineering and Laboratory for Research on the Structure of Matter, University of Pennsylvania, Philadelphia, Pennsylvania 19104

(Received 26 September 1997)

Reaction of Li with graphite at high pressures yields LiC_2, three times as dense in Li than the ambient-pressure graphite intercalation compound LiC_6. We study the stability of this unusually high Li density against Coulomb repulsion by neutron and x-ray scattering. Surprisingly, parameters which should be sensitive to interlayer interactions are quite similar to the LiC_6 values: **c**-axis compressibility $\kappa_c = 1.43 \times 10^{-12}$ cm^2/dyn, sound velocity $v_s = 5.1 \times 10^5$ cm/s, zone-boundary acoustic-phonon energy = 18.5 eV, and slightly higher thermal expansion $\alpha_c = 66 \times 10^{-6}$/K (300–450 K). Moreover, both compounds are yellow in reflection, implying that the delocalized charge densities are comparable. These and other results are consistent with partially covalent in-plane Li-Li bonds, i.e., partial charge transfer to the graphene layers, as opposed to the more conventional ionic picture which applies to most alkali-graphite intercalation compounds. [S0163-1829(98)05109-1]

I. INTRODUCTION

LiC_6 is an important prototype graphite intercalation compound (GIC) due to its simple crystal structure[1] and comparatively high metal/carbon ratio, highest of all alkali GIC's. The unit cell is hexagonal (**a**=4.305 Å, **c**=3.706 Å) and the stacking sequence is simply C/Li/C/Li. The electronic structure of LiC_6 (and other alkali GIC's synthesized at ambient pressure) derives from (nearly) complete charge transfer from alkali to the graphitic conduction band with little or no metal-carbon hybridization.[2] In-plane electrostatic repulsion limits the in-plane Li-Li distance to 4.3 Å resulting in a commensurate $\mathbf{a}(\sqrt{3} \times \sqrt{3})R30°$ superlattice. The screened Drude-like plasma frequency is 2.85 eV, well below the interband threshold,[3] thus LiC_6 appears golden yellow in reflection. Higher stage compounds LiC_{12} and LiC_{18} also exist; these are pink and blue in color, respectively.[4–6] Here too, the intercalate is essentially Li^+ and the color change from LiC_6 to LiC_{18} is associated with the downshift of the Drude edge due to reduced total charge density transferred from Li to graphene layers. The decrease in delocalized charge density with decreasing Li concentration is also reflected in the elastic properties and interlayer interactions, such as increased **c**-axis compressibilities, higher thermal expansion, and lower phonon energies.[4,7]

LiC_2, a related stage-1 high-density phase, is accessible only by high-pressure synthesis.[8,9] Volume measurements after pressure release indicate substantial metastability;[9] no rapid deintercalation of Li or swelling of the ampoule, as occurs with high-pressure reactions with heavier alkali metals (Na, K). In the ideal ''LiC_2'' structure, Li would be located over every hexagon center. X-ray-diffraction studies[10] show that LiC_2 decomposes slowly in several steps at ambient pressure, to a commensurate hexagonal cell with **a**=8.63 Å and **c**=11.1 Å $(3 \times I_c)$ and $\mathbf{a}(2\sqrt{3} \times 2\sqrt{3})R30°$ Li in-plane superlattice. A stoichiometry of Li_7C_{24} or Li_9C_{24} is observed—the unit cell is $Li_{21}C_{72}$ or $Li_{27}C_{72}$, due to three inequivalent C/Li/C layers. Both compositions correspond to the same hexagonal structure, the difference being that in the latter there are an additional two Li atoms in-plane. A dramatic enhancement is observed in the metastability of the high Li density when the graphite contains 0.5 at.% substitutional boron.[11] Average compositions from x-ray $(00l)$ intensities, determined several months after pressure release are $LiC_{2.2}$ and $LiC_{3.8}$ with and without boron, respectively. This enhanced metastability is tentatively attributed to the pinning of the superlattice by ~ 1 boron atom per cell, thus arresting the decomposition cascade.

A variety of evidence suggests that the interactions and stability energetics of LiC_2 and LiC_6 are qualitatively different. The Li density in the former exceeds that in Li metal at ambient pressure, while high-pressure studies of Li metal indicate core rehybridization and *internal* transfer of valence

electron density from $2s$ to $2p$ orbitals.[12] Pressure-induced directional 2.5 Å Li-Li bonds may be responsible for the formation of the quasiplanar Li clusters which appear to be the stable unit from which the high-order superlattices are constructed, the resulting partial covalency compensating for Coulomb repulsion. Evidence of partial Li $2p$ orbital overlap comes from IR spectroscopy[13] and ^{7}Li NMR spectroscopy.[14] The resulting localization of electronic density between Li sites reduces the charge transfer per Li atom to graphite compared to LiC_6 and nicely explains the similarity in plasma frequencies.

In this paper we study the statics (compressibility) and dynamics (phonon dispersion, thermal expansion) of interlayer interactions in high density Li-GIC's. The results summarized above suggest that, viewed as one-dimensional ionic lattices, the c-axis properties of LiC_2 and LiC_6 might be similar, whereas all previous examples [LiC_x vs x,[4] KC_8 vs KC_6 (Ref. 15)] show quantitative differences which can be simply understood in terms of electrostatic interactions which vary with (areal) charge density. Using neutron and x-ray scattering and volume vs pressure measurements, we find **c**-axis compressibility $\kappa_c = 1.43 \times 10^{-12}$ cm^2/dyn, sound velocity $v_s = 5.1 \times 10^5$ cm/s; and zone-boundary acoustic-phonon energy = 18.5 eV; all comparable to the LiC_6 values.[7,16] The thermal-expansion coefficient $\alpha_c = 66 \times 10^{-6}$/K (300–450 K) is slightly higher. The accumulated evidence thus strongly indicates that the delocalized charge densities are comparable in LiC_2 and LiC_6, with most of the additional Li $2s$ charge associated with the higher Li density in LiC_2 remaining localized analogous to the $2s \rightarrow 2p$ transfer in Li at high pressure. The interlayer potential is somewhat more anharmonic in LiC_2.

II. EXPERIMENT

High-pressure synthesis and stoichiometry characterization

Samples were synthesized using both highly oriented pyrolitic graphite (HOPG) and 0.5% boron-substituted graphite (B-HOPG) with metallic Li. 99% enriched ^{7}Li was used for the neutron inelastic experiments to minimize thermal neutron absorption. Stoichiometric amounts of Li and flat discs of HOPG or B-HOPG were placed in self-sealing stainless-steel ampoules. High-pressure synthesis was performed under quasihydrostatic conditions in an anvil apparatus using a primary double acting hydraulic cylinder with a capacity of 500 tons. The ampoule was enclosed in a graphite resistance furnace supplied by a regulated voltage that provided internal heating; the temperature was monitored with a thermocouple adjacent to the sample. Pressure was generated by compressing the ampoule within a lenticular pyrophyllite assembly placed between pressure plates. Synthesis was performed at 60 kbars and 300° C for several hours.

The samples had a light golden color; all sample handling was done in an inert argon atmosphere. Both HOPG and B-HOPG derived samples were stage 1 with repeat distances $(I_c) = 3.7$ Å similar to LiC_6.[1] Weight and volume measurements before and after synthesis confirmed the stoichiometry of the synthesized Li-GIC. The diffraction and scattering experiments were all performed at ambient pressure, so care was taken to determine the intercalated Li density at the time of measurement; Q scans yielding $(00l)$'s and $(hk0)$'s were executed at the commencement of each experiment, as done before.[11] These yielded the following results: compressibility measurement—B-$LiC_{2.3}$ and $LiC_{3.1}$; neutron inelastic phonon measurement—$LiC_{3.4}$; and thermal-expansion measurement—$LiC_{3.1}$. Here again we reconfirm, that the decomposition of the LiC_x sample based on B-HOPG is slower than that based on HOPG.

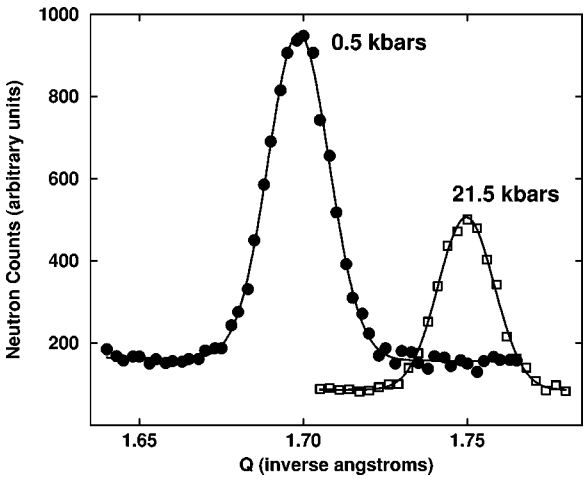

FIG. 1. Typical $00l$ ($l = 1$) elastic neutron diffractograms taken on the B-$LiC_{2.3}$ sample at 0.5 and 21.5 kbars.

III. COMPRESSIBILITY

c-axis compressibility experiments on HOPG and B-HOPG based samples were carried out *ex situ* at ambient temperature by measuring the shift in $(00l)$ Bragg positions with hydrostatic pressure. The results are compared to *in situ* volume vs pressure measurements carried out in the same apparatus used for synthesis.

A. Neutron elastic diffraction

Neutron-diffraction experiments were performed on the H4S triple-axis spectrometer at the High Flux Beam Reactor, Brookhaven National Laboratory. We used incident neutrons of 14.8 meV, pyrolitic graphite (002) monochromator and (004) analyzer and 40'-40'-40'-40' collimation.

Each sample, along with graphite which served as a pressure gauge, was wedged inside a lead plated Al capsule (6 mm diameter, 14 mm long) filled with Fluorinert FC-75 which retains fluidity to 50 kbars at 300 K and is inert with respect to LiC_x. The pressure transmitting fluid imparts no stress inhomogeneities to the compressed substance and the stress distribution can reasonably be assumed to be homogeneous. We used the McWhan-Vettier hydraulically driven pressure cell[17] consisting of a barrel-shaped cylinder of high-density polycrystalline Al_2O_3. The entire apparatus was mounted on the spectrometer table.

Elastic $(00l)$ profiles were recorded at varying pressures. $l = 1$ peaks of B-$LiC_{2.3}$ at the pressure limits are shown in Fig. 1. Above 21 kbars severe degradation of the mosaic and reduction in peak intensity was observed, indicating crushing of the sample due to physical contact with the cell walls. The experiment was halted at this point and ambient pressure $(00l)$'s were rerecorded. The lattice constants were completely reproducible.

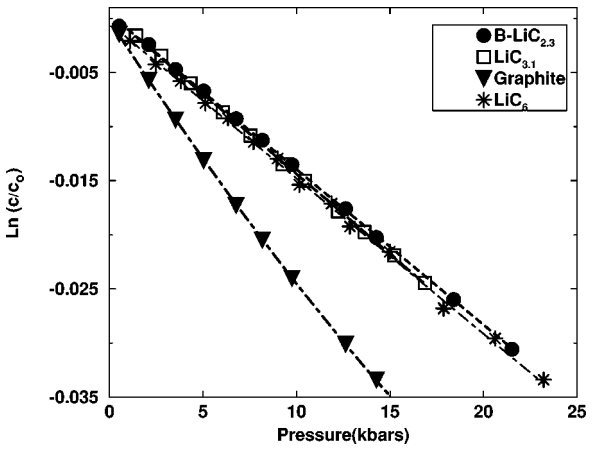

FIG. 2. Neutron-diffraction data show the variation of $\ln(c/c_0)$ vs pressure (in kbars). Linear fits are shown for B-$LiC_{2.3}$, ($\mathbf{c}_0 = 3.70$ Å); $LiC_{3.1}$, ($\mathbf{c}_0 = 3.69$ Å), and LiC_6, ($\mathbf{c}_0 = 3.701$ Å); quadratic fit for HOPG, ($\mathbf{c}_0 = 3.354$ Å).

Calibration of the hydraulic press was done by measuring the graphite c parameter over the same pressure range and fitting to an empirical nonlinear relationship established by x-ray diffraction:[18]

$$\frac{c}{c_0} = \left[\left(\frac{\zeta'}{\zeta_0} \right) P + 1 \right]^{-1/\zeta'}, \tag{1}$$

where c_0 is the ambient pressure c parameter = 3.354 Å, ζ_0 is the c-axis compliance = 360 kbars, and ζ' is its dimensionless pressure derivative = 10. Normalized c parameters vs pressure are plotted in Fig. 2. Ambient pressure $\mathbf{c}_0$ parameters were determined from Gaussian fits to Bragg ($00l$) reflections, yielding $\mathbf{c}_0 = 3.69$ Å for B-$LiC_{2.3}$ and $LiC_{3.1}$ ($l = 1,2$) and $\mathbf{c}_0 = 3.354$ Å for graphite ($l = 2,4$).

The relation between c and pressure is observed to be essentially linear for B-$LiC_{2.3}$ and $LiC_{3.1}$, in contrast to the proven polynomial behavior in graphite.[18] Accounting for experimental uncertainties, a linear least-squares fit gives a satisfactory result and yields a constant c-axis isothermal compressibility shown in Fig. 2, i.e.,

$$\kappa_c = \frac{d(\ln(C/C_0))}{dP}. \tag{2}$$

The maximum departure from linearity was estimated by fitting to a polynomial

$$\ln\frac{c}{c_0} = \kappa_0 - \kappa_c' P - \kappa_c' \frac{P^2}{2}, \tag{3}$$

and extracting the quadratic term. The results are compared in Table I.

The quadratic component of the fit does not show significant deviation over the pressure range for both samples. Thus, the linear fit describes the entire pressure range quite accurately within the established error bars—$\kappa_c = 1.44 \pm 0.03 \times 10^{-12}$ cm^2/dyn for B-$LiC_{2.3}$ between 0.5 and 21 kbars; $\kappa_c = 1.48 \pm 0.08 \times 10^{-12}$ cm^2/dyn for $LiC_{3.1}$, between 1.5 and 17 kbars. In comparison, $\kappa_c = 1.43 \pm 0.02 \times 10^{-12}$ cm^2/dyn for LiC_6.[7] In contrast, the data shows that graphite becomes notably nonlinear in the same pressure range, with a compressibility that agrees with the accepted value, $\kappa_c = 2.79 \pm 0.1 \times 10^{-12}$ cm^2/dyn.[19]

TABLE I. Compressibility values calculated from the linear fit and from the pressure limits of the quadratic fit. In both cases, the linear fit suffices to describe the entire pressure range.

	Compressibility (10^{-12} cm^2/dyn)		
Fit	B-$LiC_{2.3}$	$LiC_{3.1}$	LiC_6 (Ref. 7)
Linear	1.44 ± 0.03	1.48 ± 0.08	1.43 ± 0.01
Quadr (lower)	1.47 (0.5 kbars)	1.55 (1.4 kbars)	
Quadr (upper)	1.40 (21 kbars)	1.40 (17 kbars)	

B. Pressure-volume experiments for κ_c

The c-axis compressibility should also be accessible from $V(P)$ measurements since the bulk modulus is dominated by the soft interlayer direction. Such measurements are readily performed in the same apparatus as is used for synthesis, the drawback being that only the global C/Li ratio is known (from weighing the materials loaded into the ampoule). Such experiments were performed on ''samples'' predetermined to be $LiC_{2.5}$ and LiC_3; the results are shown in Fig. 3. The $P(V)$ behavior can be broken into two segments to better understand the mechanism in the piston-cylinder experiment.

Since LiC_2 is unstable at ambient pressure, the contents of the ampoule will undergo some deintercalation upon completion of synthesis and release of pressure. Thus at the beginning of the compressibility experiment at $P = 1$ atm, there is some free Li present along with LiC_x. This results in an artificially large apparent initial compressibility (2.07×10^{-12} dyn^2/cm) in the first segment (between 1 and 5 kbars) due to the very high compressibility of Li metal, 7.01×10^{-12} dyn^2/cm, *and* the volume decrease accompanying the reintercalation of Li with increasing P. At higher pressures the apparent compressibility drops as the free Li is consumed, resulting in a lower and more reliable value from

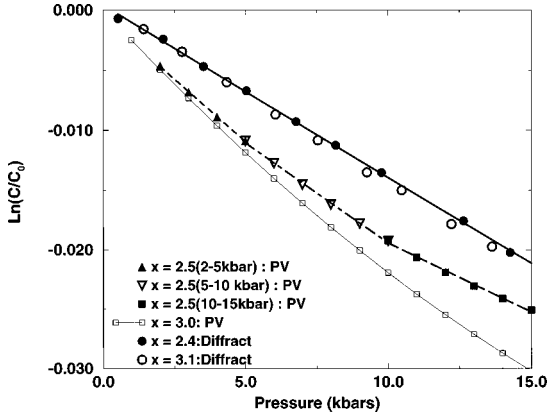

FIG. 3. Pressure-volume (PV) data from piston-cylinder experiment compared with neutron diffraction. PV data are divided into two segments (see text). κ_c ($LiC_{2.5}$, linear fits to PV data) in different pressure ranges: 2.07 (2–5 kbars), 1.72 (5–15 kbars); κ_c (linear fits to neutron data) is 1.44 (B-$LiC_{2.3}$) and 1.48 ($LiC_{3.1}$): all in 10^{-12} dyn^2/cm units.

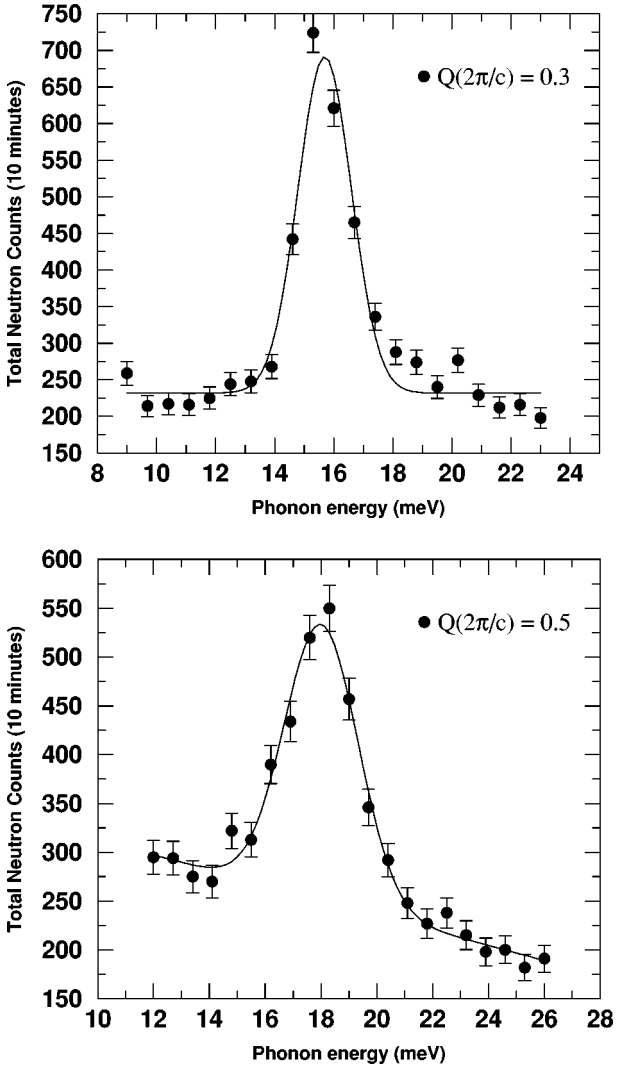

FIG. 4. Typical constant q ($q=0.3$ and 0.5 Å^{-1}) scans representing phonon groups of the $(00l)$ longitudinal-acoustic mode for $LiC_{3.1}$.

5 to 15 kbars, $\kappa_c=1.72\times10^{-12}$ dyn^2/cm for $LiC_{2.5}$. This is in better agreement with the diffraction-derived result, and confirms the fact that the large increase in in-plane density has at most a minor effect on κ_c. Similar deintercalation-intercalation phenomena were observed in the neutron-diffraction compressibility experiments. As expected, the effect was smaller in the B-HOPG sample since less Li deintercalates in a given time after pressure release compared to HOPG.

IV. PHONON-DISPERSION SPECTRA

A. Neutron inelastic experiments

The neutron inelastic experiments were carried out at the H4S triple-axis spectrometer at the High Flux Beam Reactor, Brookhaven National Laboratory and at National Bureau of Standards Reactor, National Institute of Standards and Technology.

PG(002) monochromator and analyzer were used, with an incident energy of 14.8 meV. The geometry was chosen to measure longitudinal $(00l)$ phonons; these are characterized by the vibrations of the C/Li planes with displacement and propagation vector along the c axis.

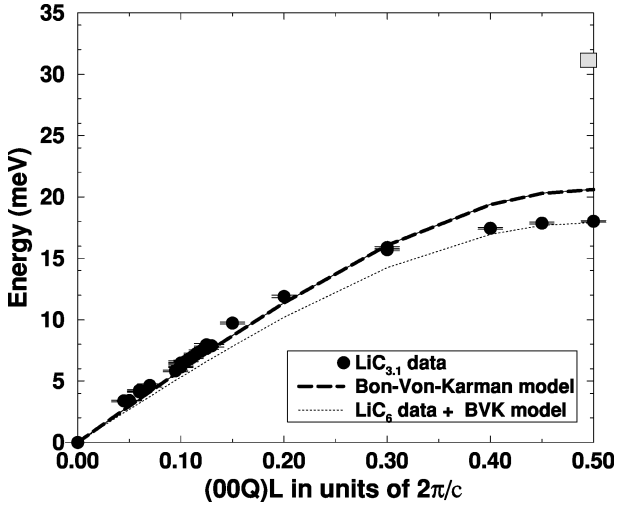

FIG. 5. Phonon dispersion for $(001)l$ modes in $LiC_{3.1}$. Experimental data are shown by filled circles and error bars. Best fit Born–Vón Kármán models for $LiC_{3.1}$ and LiC_6 are also plotted.

All phonon scans were reproducible, verified in two separate measurements done at both reactors, as well as under different conditions such as fixed monochromator/analyzer energy. The ''sample'' consisted of four unopened high-pressure ampoules (containing $LiC_{3.1}$) lined up vertically, in an attempt to maximize detected signal. Phonon groups measured at 300 K in constant q scans of the $(00l)$ longitudinal-acoustic mode are plotted in Fig. 4. The phonon polarization was verified to be $(00q)l$, by rotating the (001) axis by 90° in the scattering plane.

The c-axis dispersion of the longitudinal modes is shown in Fig. 5; wave vector q is plotted in units of $2\pi/c$, where c is the repeat distance = 3.7 Å. The data have been analyzed in two parts: the low q, acoustic behavior yields sound velocities and elastic constants to be compared with values obtained directly from diffraction data, and a lattice-dynamical model has been fit to the data in an attempt to obtain interlayer force constants.

B. Analysis from $q\rightarrow0$ data

The low-frequency data exhibit linear behavior $\omega\sim q$ as $q\rightarrow0$; the slope $\Delta\omega/\Delta q$ of this line yields a sound velocity, $V_s=5.08\times10^5$ cm/s. Subsequently, we can evaluate the elastic constant, $C_{33}=6.64\times10^{11}$ dyn/cm^2, as $C_{33}=V_s^2\cdot\rho$, where ρ is the mass density of the sample ($=2.57$ g/cm^3).

The formula for the elastic modulus B_c in terms of the elastic stiffness constant is

$$B_c=X(C_{11}+C_{12}-2C_{13})^{-1}, \tag{4}$$

where

$$X=C_{33}(C_{11}+C_{12})-2(C_{13})^2. \tag{5}$$

Additionally,

$$B_c=\frac{1}{\kappa_c}. \tag{6}$$

TABLE II. Comparison of C_{33} from neutron elastic diffraction and longitudinal acoustic (LA) low-frequency phonon studies. There is very good agreement between the C_{33} values obtained from the two experiments, for $LiC_{3.1}$. Additionally, the agreement for LiC_6 is also excellent, compared to previous work.

	$C_{33}\times10^{11}$(dyn/cm^2)	
	Neutron diffraction	LA phonon dispersion Low Q data
$LiC_{2.4}$	6.97	
$LiC_{3.1}$	6.76	6.64
LiC_6	6.97	6.93 (this work), 8.9 (Ref. 16), 7.1 (Ref. 7)

Because of the strong coplanar covalent bonds in pristine and intercalated graphite, the compression of the a-axis spacing is negligible and we can assume that C_{13} is essentially zero. So, to a good approximation, $C_{33}\sim1/\kappa_c$. We obtain a value for $\kappa_c=1.51\times10^{-12}$ cm^2/dyn. This compares very favorably to the compressibility values calculated from the neutron elastic diffraction in the previous section ($\kappa_c=1.48\times10^{-12}$ cm^2/dyn and 1.44×10^{-12} cm^2/dyn). Phonon-dispersion data of LiC_6 were also taken as a comparison and we obtained $C_{33}=6.93\times10^{11}$ dyn/cm^2 and $\kappa_c=1.44\times10^{-12}$ cm^2/dyn from the low-q data. This is tabulated in Table II.

C. Lattice-dynamical model

Attempts to fit the $(00q)l$ acoustic modes obtained for $LiC_{3.1}$ with a simple Born–vón Kármán force-constant model and the one-dimensional ion shell model used by Zabel *et al.*[16] for LiC_6 were made, by simply scaling the Li density in the GIC; the models essentially consist of an assembly of rigid layers connected by Hooke's law springs. The ''best-fit'' model shown in Fig. 5 yields a rough estimate of ϕ_{ic} (interplanar force constant between Li-C rigid layers along the c axis) = 9850 ± 1000 dyn/cm per carbon atom, to be compared with $\phi_{ic}(LiC_6)=7445$ dyn/cm.[19] However, the discrepancy between the model and data is evident and the absence of the experimental optic branch makes the fit unreliable. Attempts at measuring the optic branch were not successful here due to the low scattering volume and high sample mosaic ($\sim15°$), hence a complete lattice dynamical analysis is not possible.

The salient features of the experimental data are (1) the qualitative similarity in the $00l$ longitudinal-acoustic dispersion between ''LiC_2'' and LiC_6,[16] (2) the zone-edge phonon energy, $E_z=18.5$ meV is the same as in LiC_6,[16] (3) the long-wavelength limit calculations of v_s, C_{33}, and κ_c agree very well with direct compressibility measurements from diffraction in the previous section, (4) the notable inadequacy of the Born–vón Kármán model to describe the interlayer interactions, in light of its success with all other alkali-GIC's; all this will be discussed later in more detail.

V. c-AXIS THERMAL EXPANSION

The thermal-expansion experiment was carried out on the RIGAKU diffractometer using x-ray Cu $K\alpha$ radiation ($\lambda=1.54\,056$ Å). The sample was mounted on the surface of a micro-miniature refrigerator (MMR); the MMR is a Joule-Thompson refrigerator, that uses a Pt resistor as a temperature sensor, and operates over a wide range of temperatures. $00l$ ($l=1,2$) reflections between 100 and 400 K were recorded; Fig. 6 shows the variation of c with temperature for $LiC_{3.1}$ and LiC_6.

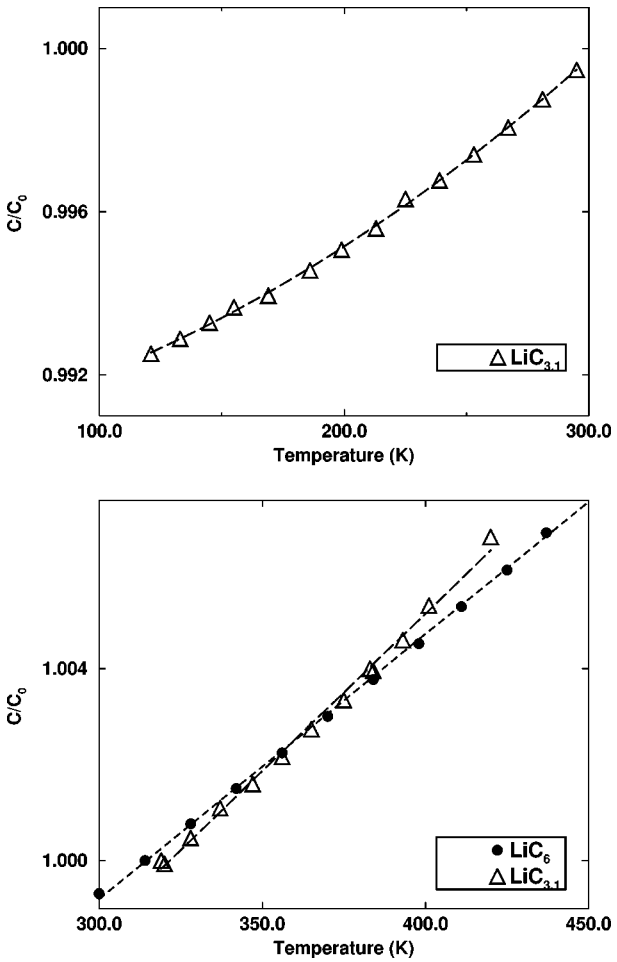

FIG. 6. Thermal-expansion data for LiC_6 and $LiC_{3.1}$ from Gaussian fits to x-ray $(00l)$'s. 300 K c parameters were 3.695 and 3.685 Å, respectively. Solid lines are quadratic (100–300 K) and linear (300–450 K) fits to the data.

The c-axis thermal-expansion coefficient α_c is defined as

$$\alpha_c=\frac{1}{c}\frac{dc}{dT}, \tag{7}$$

where c is the c-axis lattice constant at 300 K. c is observed to increase with a quadratic (concave) curvature from 100 to 300 K, and follows an essentially linear increase above room temperature until 450 K (Fig. 6).

The best fit of the low-temperature data is with a quadratic function, shown in Fig. 6(a); the slope is evaluated at an average temperature and α_c is calculated. The high-temperature data is fit best to a straight line, shown in Fig. 6(b). The calculated values of α_c are tabulated in Table III.

For $LiC_{3.1}$, in the linear region between 200 and 300 K, $\alpha_c=46\times10^{-6}$/K. In comparison $\alpha_c=31\times10^{-6}$/K (Ref. 20) for LiC_6. The heating curves from 300 to 450 K yield $\alpha_c=66\pm1.5\times10^{-6}$/K for $LiC_{3.1}$ and 55×10^{-6}/K for

TABLE III. Thermal-expansion values for Li_xC_6.

LiC_x	α_c (10^{-6} /K)			
$LiC_{3.1}$	66 ± 1.5	(300–450 K);	46 ± 1	(200–300 K)
LiC_6	55 ± 1	(300–450 K);	31 (Ref. 20)	(200–300 K)
$Li_{0.89}C_6$	76 (Ref. 7)	(450–650 K)		
$Li_{0.69}C_6$	110 (Ref. 7)	(450–650 K)		

LiC_6. The values of α_c for LiC_6 and the dilute phases $Li_{0.89}C_6$ and $Li_{0.69}C_6$ (Ref. 7) are tabulated in Table III. It is notable that with reducing Li density in the ambient pressure GIC's, the c-axis thermal expansion (α_c) gets larger. This arises from the enhanced thermal amplitude of effectively ''lighter'' ions. The obvious discrepancy of this picture with $LiC_{3.1}$, in light of its larger thermal expansion (compared to LiC_6), is discussed later.

The anharmonicity in the potential can be quantified by calculation of the Grüneisen parameter (γ), studied in a one-dimensional (1D) quasiharmonic approximation, where $\gamma = \alpha V/\kappa_T C_v$ for the simplest case. α is the 1D thermal expansion and κ_T is the isothermal compressibility. We estimate a value close to the Dulong-Petit value of $C_v = 3k_b$ for ambient temperatures and for a system with 3 degrees of freedom. Along the c axis, the ideal theoretical case is $C_v = 2k_b$. However, guided by previous work,[7] the experimental value obtained from the phonon spectra is less than that and in the particular case of LiC_6 is $1.6k_b$.[7] Taking the unit-cell volume as $V=(\sqrt{3}/4)a^2c$, where $a=2.46$ Å and $c=3.7$ Å, and the experimental values of α and κ_T, we obtain $\gamma=1.96$ for the $LiC_{3.1}$ sample. This number is slightly larger than that for LiC_6 ($\gamma=1.80$).[7]

VI. DISCUSSION

The most interesting property of these high-pressure compounds is the nature of the intercalated alkali state that permits the stabilization of such high Li densities within graphite under high pressure. The above experiments lead to some very interesting conclusions that have been discussed individually with respect to elastic properties and charge transfer, inter-layer force constants, and overall potential anharmonicity.

A. Elastic properties and charge transfer

In LiC_6, (and other alkali GIC's), the interlayer coupling is described as a partially screened Coulomb interaction, mediated by (nearly) complete valence electron transfer from the donor to the graphite conduction band, thus making the bonding essentially ionic in character. It is semiquantified in view of experimental data as

$$\kappa_c \sim \frac{1}{\sigma^2}, \tag{8}$$

where σ is alkali charge *transfer* as opposed to charge *density* as in (Ref. 4). Woo *et al.*[4] used a simple model where the total elastic energy (E_T) has a contribution from the C layers and electrostatic energy ($E_{\rm es}$) of the C/I/C sandwich. $E_{\rm es} = A_o\sigma_o^2 c_i$; σ is the areal charge density per unit area, A_0 is the area per atom, and c_i is the c-axis repeat distance. Compressibility of the C/I/C sandwich is $\kappa_i = (A_o/c_i)(d^2E_T/dc_i^2)^{-1}$, where $(d^2E_T/dc_i^2) = (1/3c_i) \times (dE_{\rm es}/dc_i)$. This yields $\kappa_i \sim 1/\sigma^2$. The dilute phases, LiC_{12} and LiC_{18} show a progressive increase in compressibilities (compared to LiC_6), reflecting the decreased total charge transfer from the Li to the C layer.[4]

The experiments done above yield compressibility values κ_c (or equivalently C_{33}) for B-$LiC_{2.3}$ and $LiC_{3.1}$. These are observed to be exactly the same as in LiC_6, Table II: $\kappa_c \sim 1.43\times10^{-12}$ cm^2/dyn in B-$LiC_{2.3}$, $LiC_{3.1}$, and LiC_6, in spite of the enhanced Li density in the former two compounds. This is in striking contrast to the dilute phases mentioned above. From Eq. (8), this reflects similar *total* charge transfer along the c axis from the Li layer to C in the three GIC's, and hence similar Li-C interplanar coupling constants. Additionally, the initial slope of the acoustic $(00l)$ branch is a direct measure of the elastic constant, C_{33}. The results show that there is excellent agreement between the C_{33} values obtained from the neutron elastic and inelastic (long-wavelength limit) experiments.

These results support and reinforce the picture of the extra charge density in ''LiC_2'' being localized near the Li core, resulting in *reduced electron transfer per Li atom to C*, and hence *similar total charge transfer from the Li layer to C* in B-$LiC_{2.3}$/$LiC_{3.1}$ as LiC_6.

This is consistent with the scenario proposed earlier, as follows. High pressure favors the partial transfer of electrons from the $2s$ to the more localized $2p$ orbital accompanied by essential alkali metal volume decrease in Li metal.[12] This picture carried over to LiC_2, forces the Li atoms closer together and $2p$ orbital overlap leads to the formation of short covalent Li-Li ''bonds,'' permitting near-neighbor occupancy of Li over graphite hexagons. The rest of the Li $2s$ charge is transferred to the carbon layer, *this* total charge transfer being similar to that in LiC_6.

Hence, the perception of the intercalated Li state in ''LiC_2,'' electronically and physically, is that the total charge density is distributed between Li-Li in-plane bonds (some electrons are in localized, radially smaller $2p$ orbitals) and Li-C out-of-plane bonds (electrons are in delocalized, hybridized Li $2s$ and C π orbitals $\sim$ LiC_6).

Evidence of similar charge transfer in the two compounds also arises from another source. It is known[21,22] that if electrons are donated by the intercalate to the graphitic layer, the Fermi level E_f is raised in the carbon p_z (or π) band; reflected in a measurable dilation of the in-plane C-C bond length. This has been confirmed from x-ray diffraction in work described in Ref. 23, which yields similar C-C bond lengths of 1.438 ± 0.001 Å for B-$LiC_{2.2}$ and $LiC_{3.1}$, very close to 1.436 Å for LiC_6. In contrast the C-C bond length for graphite is 1.42 Å.

B. Phonon dispersion and lattice dynamics

Attempts to analyze the phonon-dispersion data for $LiC_{3.1}$ were made with a typical Born–vón Kármán model. This was motivated by its successful application to the lower graphitelike acoustic branches in LiC_6 and other alkali-GIC's.[24,25] The least-squares fit shown in Fig. 5 is not

very good, indicating that the data cannot be perfectly represented by the Born–vón Kármán (BvK) model at high-q values. Several n-parameter ($2 \leqslant n \leqslant 6$) BvK models were tested; consideration of longer-range force constants between successive Li-Li, C-C, and Li-C planes did not significantly improve the fit quality. Probably, with a large enough number of force constants, the acoustic-phonon branch could be reproduced; however, the physical interpretation of this model may not be useful. Its failure in this case allows a qualitative physical description of the interactions, implying that a more complicated elastic and electrostatic interaction needs to be considered for $LiC_{3.1}$; the ion shell model (all Li atoms being treated as hard spheres) not satisfactorily describing the electronic interactions. This brings up two points: (a) The presence of in-plane high-density Li clusters in $LiC_{3.1}$ might create puckered intercalate layers and hence a deformation of the C host layers, rendering the rigid-plane model insufficient. By considering the local strain that is generated around isolated clusters (instead of atoms) and its effect on both inter- and intralayer interactions, the elastic and vibrational energetics might be more accurately estimated; (b) In view of the charge-transfer model described in the previous subsection, one should consider the different physical attributes of the partially filled s and p orbitals and their elastic interactions. A complete calculation of these effects would require comparison to the experimental optic branch and the layer bending modulus. Attempts at measuring the optic branch were not successful for reasons mentioned earlier; hence these detailed calculations were not carried out.

However, the present data, in the absence of a detailed model, provide a great deal of insight into the c-axis bonding in $LiC_{3.1}$. A zone-boundary acoustic-phonon energy, $E_{za} = 18.5$ meV (Fig. 5) is observed for $LiC_{3.1}$, similar to that in LiC_6.[16] The linear chain, Born–vón Kármán model predicts the relation: $E_{za} \sim \sqrt{2\phi_{ic}/M_c}$, where ϕ_{ic} is the interplanar Li-C force constant and M_c is the mass of the carbon layer. From this, we evaluate $\phi_{ic} = 7926$ dyn/cm for $LiC_{3.1}$, to be compared with 7445 dyn/cm for LiC_6.[16] This enables us to make two predictions concerning the acoustic and the optic branch. The acoustic branch is determined by the vibration of the carbon layers, whereas the optic branch depends on the intercalate (Li) layers. Additionally, it is known that the interlayer force constant is primarily dependent on the intercalate mass density and the interlayer spacing.[16] Due to the similarity in interlayer spacing (3.7 Å) between LiC_6 and $LiC_{3.1}$ and the twofold increase in Li density in $LiC_{3.1}$, one would expect the acoustic zone-edge energy to be a few meV's lower in the latter, arising primarily due to the effect of the increased intercalate mass on the vibration of the carbon layers. This is notably not observed here, giving rise to similar force constants for both compounds. Of course, the optic branch is required to unequivocally determine ϕ_{ic}. The calculated value of ϕ_{ic} from the acoustic branch, however, can be used to predict the placement of the optic branch zone edge from $E_{zo} \sim \sqrt{2\phi_{ic}/M_{Li}}$, where M_{Li} is the mass of the lithium layer. This predicts an energy, $E_{zo} = 34$ meV in $LiC_{3.1}$. Tentative inelastic experiments done at NIST indicate an optic zone-edge energy at $E_z = 30.7 \pm 0.5$ meV in $LiC_{3.1}$, measured at $(hkl = 0,0,2.5)$ with incident neutron energy 14.7 meV, in excellent agreement with the above prediction. The same calculation, with the same force constant, predicts $E_{zo} = 59$ meV for LiC_6. Zabel *et al.*[16] have experimentally observed $E_{zo} = 60$ meV in LiC_6, for the optic zone edge energy, again in excellent agreement with the calculation. Additionally, due to the increased Li density in $LiC_{3.1}$, one would expect a relatively dispersionless branch in the latter, compared to LiC_6.

Thus, from the qualitative similarity of the acoustic branch, the similarity in zone-edge acoustic phonon energies (18.5 meV), the predicted optic branch energy (34 meV) along with tentative experimental support for the optic branch zone-edge energy (30.7 meV), we conclude that the interlayer force constant (ϕ_{ic}) in LiC_6 and $LiC_{3.1}$ are the same (~ 7500 dyn/cm). This implies similar Li-C bonding, supporting the idea of a similar degree of *total ionization/charge transfer to C* of Li, in spite of the large Li density difference. This again points to similar c-axis energetics and interactions and different in-plane chemistry. The long-wavelength limit calculations of v_s, C_{33}, and κ_c obtained from the linear slope and their excellent agreement with direct neutron elastic diffraction measurements have already been discussed in the context of charge transfer.

C. Anharmonicity

The thermal-expansion experiments on $LiC_{3.1}$ and LiC_6 (Table III) indicate greater thermal expansion (and hence anharmonicity) in the dense and dilute phases compared to LiC_6. A semiharmonic potential has a vibration frequency:

$$\omega \sim \sqrt{k/m}, \tag{9}$$

that scales inversely with mass. As the ''effective'' mass of the Li layers gets lighter, one samples the higher part (higher frequency) of the potential and the thermal amplitude gets larger. This accounts for a larger α_c for $Li_{0.69}C_6$ as compared to LiC_6.

However, in $LiC_{3.1}$, the intercalate layers are ''heavier'' and if the potential, $V(r)$, were the *same*, we should sample lower frequencies ω and the thermal expansion α_c should decrease. The experimental results however are contrary; so one can imagine a different scenario for $LiC_{3.1}$ (schematic in Fig. 7). A potential that has *greater* anharmonicity than in LiC_6, is proposed. In this picture, the ''heavier'' layers in $LiC_{3.1}$ sample the lower portion of the potential and still have a larger thermal amplitude, in accordance with the more nonparabolic potential. This can be attributed to contributions from two sources and contrasted from the typical ionic vibration observed in LiC_6. The metastable in-plane Li clusters would have lower-frequency vibrational modes, as they are heavier and relatively more immobile. On the other hand, the intracluster modes representing the individual modes of the Li atoms would have higher frequency than the ionic vibration in LiC_6. The combination of these suggest an overall greater thermal amplitude in $LiC_{3.1}$ and one can assign to the Li clusters, a shallow (broad) potential well as opposed to the deep (corrugated) potential well for the (stable and fixed) Li ions in LiC_6.

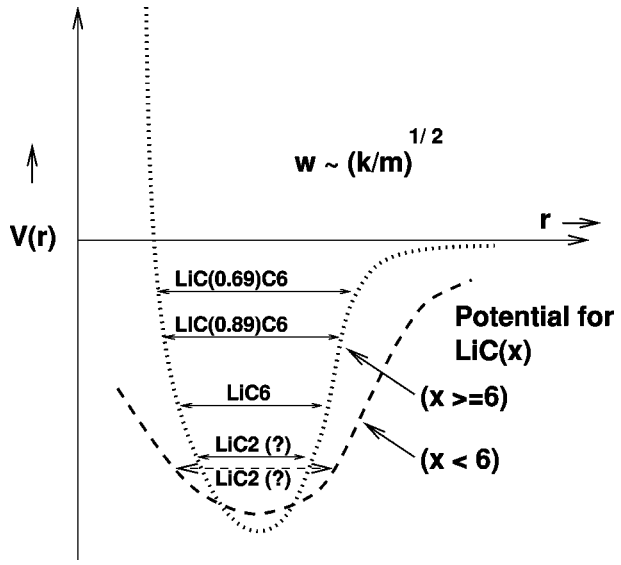

FIG. 7. Potential for LiC_x: this is shown for $x>6$ and $x<6$. See text for details.

This result is consistent with the similarity in C_{33}, even though α_c is different in LiC_6 and LiC_2. This is understandable, as C_{33}, unlike α_c, is reflective more of the elastic and electrostatic interactions between the layers and not so much with the overall ''parabolicity'' of the potential. In the lattice-dynamical properties, both the lattice stiffness and the phonon anharmonicity have an important effect on the c-axis lattice expansion: where an increase in the lattice stiffness reduces the c-axis lattice expansion, and an increase in the anharmonicity enhances the lattice expansion.

VII. SUMMARY

We conclude from the above results, that taken as a 1D ionic lattice, the interlayer interactions in LiC_6 and LiC_2 are similar, despite the difference in potential that might have been expected due to the threefold difference in Li density if Li was completely ionized. These experiments produce similar repeat distances, c-axis compressibilities, sound velocities and longitudinal-acoustic phonon dispersion and slightly higher thermal-expansion values. More specifically, this implies that the *total* charge transfer from the Li layer to C is the same in LiC_6 and LiC_2, i.e., the charge transfer per Li to C is incomplete in LiC_2. This offers indirect evidence for and is consistent with the picture of the extra Li valence charge being localized at the Li layer in LiC_2. Earlier spectroscopic evidence[13,14] suggest similar delocalized charge densities in both compounds. High-pressure studies[12] on Li metal indicate pressure-induced partial electronic transfer of the $2s$ valence charge to the $2p$ orbital, which becomes energetically favorable under high pressure. This localized charge in LiC_2 creates stable quasiplanar Li_7 clusters between the graphene layers through $2p$ orbital overlap, with 2.46 Å Li-Li bonds. This scenario of the intercalated Li state could explain the stabilization of the high Li density in LiC_2 against Coulomb repulsion, which is thought to be the factor limiting the Li density in LiC_6.

Additionally, the experiments above yield further evidence for interlayer interactions. The longitudinal-acoustic phonon dispersion spectra yield similar interplanar force constants for LiC_2 and LiC_6, emphasizing that the Li-C c-axis bonding is similar; the Li clusters however probably lead to the deformation of the C host layers. Thermal-expansion studies yield a slightly larger α_c for LiC_2, indicating greater anharmonicity in the potential. As already mentioned earlier, the similarity in colors also indicates similar delocalized charge, aside from interband transitions. LiC_6 is yellow in reflection with a screened Drude plasma frequency is 2.85 eV.[26] LiC_2 remains pale yellow; if the delocalized π charge scaled with Li density, it would be colorless and emit a 5 eV plasmon.

ACKNOWLEDGMENTS

This work was supported by the Department of Energy, DE-FC02-86ER45254 and by NATO Linkage Grant No. 921350, and made use of MRSEC Shared Experimental Facilities supported by the National Science Foundation under award No. DMR96-32598. Synchrotron and neutron facilities at Brookhaven are supported by DOE Basic Energy Sciences, DEAC02-76CH00016. We are very grateful to Ingvey Fei and Michael Walter for help with the high pressure synthesis at the Geophysical Laboratory, Carnegie Institution, and to Arthur Moore, Advanced Ceramics Corp., for the gifts of HOPG and and B-HOPG.

[1] D. Guérard and A. Herold, Carbon **13**, 337 (1975).
[2] N. A. W. Holzworth, S. G. Louie, and S. Rabii, Phys. Rev. B **30**, 2219 (1984).
[3] L. A. Grunes, I. P. Gates, J. J. Ritsko, E. J. Mele, D. P. DiVincenzo, M. E. Preil, and J. Fischer, Phys. Rev. B **28**, 6681 (1983).
[4] K. C. Woo, W. A. Kamitakahara, D. P. DiVincenzo, D. S. Robinson, H. Mertwoy, J. W. Milliken, and J. E. Fischer, Phys. Rev. Lett. **50**, 182 (1983).
[5] P. Plufger, K. P. Ackermann, R. Lapka, E. Schupfer, P. Jeker, H. Guntherodt, E. Cartier, and F. Heinrich, Synth. Met. **2**, 285 (1980).
[6] S. B. DiCenzo, S. Basu, and G. K. Wertheim, Synth. Met. **3**, 139 (1980).
[7] P. Zhou and J. E. Fischer, Phys. Rev. B **53**, 12 643 (1996).
[8] K. N. Semenenko, V. V. Avdeev, and V. Z. Mordkovich, Dokl. Akad. Nauk SSSR **271**, 1402 (1983).
[9] V. V. Avdeev, V. A. Nalimova, and K. N. Semenenko, High Press. Res. **6**, 11 (1990).
[10] V. A. Nalimova, D. Guérard, M. Lelaurain, and O. V. Fateev, Carbon **33**, 177 (1995).
[11] V. A. Nalimova, C. Bindra, and J. E. Fischer, Solid State Commun. **97**, 583 (1996).
[12] J. C. Boettger and R. C. Abera, Phys. Rev. B **39**, 3010 (1989).
[13] V. A. Nalimova, G. N. Bondarenko, V. L. Kofman, V. V. Avdeev, and K. N. Semenenko (unpublished).
[14] J. Conard, V. A. Nalimova, and D. Guérard, Mol. Cryst. Liq. Cryst. Sci. Technol., Sect. A **244**, 35 (1994).
[15] C. D. Fuerst, J. E. Fischer, J. D. Axe, J. B. Hastings, and D. B.

McWhan, Phys. Rev. Lett. **50**, 357 (1983).
[16] H. Zabel, A. Magerl, and J. J. Rush, Phys. Rev. B **27**, 3930 (1983).
[17] D. B. McWhan, C. Vettier, R. Youngblood, and G. Shirane, Phys. Rev. B **20**, 4612 (1979).
[18] M. Hanfland, H. Beister, and K. Syassen, Phys. Rev. B **39**, 12 598 (1989).
[19] H. Zabel and S. A. Solin, *Graphite Intercalation Compounds* (Springer-Verlag, New York, 1990), Vol. 1.
[20] J. Conard, P. Languine, H. Estrade-Szwarckopf, G. Hermann, D. Guérard, and P. Lagrange, Physica B & C **105**, 285 (1981).
[21] R. Moret, in *Intercalation in Layered Materials*, NATO ASI Series B: Physics, edited by M. S. Dresselhaus (Plenum, New York, 1986), Vol. 148, p. 185.
[22] L. Pietronero and S. Strassler, Phys. Rev. Lett. **47**, 593 (1981).
[23] C. Bindra, V. A. Nalimova, and J. E. Fischer, Mol. Cryst. Liq. Cryst. Sci. Technol., Sec. A (to be published).
[24] S. E. Hardcastle and H. Zabel, Phys. Rev. B **27**, 6363 (1983).
[25] H. Zabel and A. Magerl, Phys. Rev. B **25**, 2463 (1982).
[26] L. A. Grunes, I. P. Gates, J. J. Ritsko, E. J. Mele, D. P. DiVincenzo, M. E. Preil, and J. E. Fischer, Phys. Rev. B **28**, 6681 (1983).